ELSEVIER

Journal of Nuclear Materials 289 (2001) 199–203

journal of nuclear materials

www.elsevier.nl/locate/jnucmat

Optical emission due to ionic displacements in alkaline earth titanates

R. Cooper [a], K.L. Smith [b,*], M. Colella [b], E.R. Vance [b], M. Phillips [c]

[a] *Department of Chemistry, University of Melbourne, Parkville, Vic. 3052, Australia*

[b] *Materials Division, Australian Nuclear Science and Technology Organisation, P.M.B. 1, Menai, NSW 2234, Australia*

[c] *Department of Applied Physics, University of Technology, Sydney, P.O. Box 123, Broadway, NSW 2007, Australia*

Abstract

Optical emission spectra in the 300–700 nm range were collected from single crystal $CaTiO_3$, $SrTiO_3$ and $BaTiO_3$, and polycrystalline $CaTiO_3$ samples, that were irradiated at room temperature using a Febetron 706 variable energy pulsed-electron-beam generator. The long-lived emissions (up to microseconds after the electron pulse) consist of broad (halfwidths ~100 nm) bands centred around 380, 425, and 445 nm for $CaTiO_3$, $SrTiO_3$ and $BaTiO_3$, respectively. These emission bands are similar to cathodoluminescence emissions from 25 keV electron irradiation attributed by others to direct conduction-valence band transitions in unreduced samples and oxygen vacancies in reduced samples. $CaTiO_3$, $SrTiO_3$ and $BaTiO_3$ all have emission thresholds of 0.26 ± 0.02 MeV. This corresponds to a threshold displacement energy for oxygen, E_d of 45 ± 4 eV.

PACS: 61.72.Ji; 61.80.Fe; 61.82.Fk

1. Introduction

Perovskite, $CaTiO_3$, is a key phase in some varieties of Synroc [1], a family of titanate ceramics designed for high-level radioactive waste immobilisation. The waste contains actinide ions that, when incorporated in the crystalline Synroc, give rise to lattice damage, primarily from the alpha-recoil nucleus of mass ~210–240 amu and energy ~80–100 keV. Approximately 1500 atoms are displaced in each event [2]. Hence perovskite (and other phases) in Synroc is prone to structural disordering from radiation damage. These effects have been evidenced in X-ray diffraction studies of Synroc doped with the short-lived actinide emitters Cm-244 [3] and Pu-238 [4]. Lattice damage effects have also been observed in heavy-ion irradiation [5,6] of perovskite, using transmission electron microscopy (TEM). However there is currently no information on the identity of the radiation-induced fundamental point defects in $CaTiO_3$.

Various techniques have been used to monitor defect production and/or expose the presence of pre-existing defects in irradiated non-metals. In principle, displaced ions can be detected directly using high resolution TEM. However difficulties associated with sampling and matching of simulated to experimental images make its application impractical. TEM can be used at lower resolution to detect aggregates of point defects such as dislocation loops. Rutherford back scattering on single crystals can be used to detect displaced ions, which have formed interstitials that severely interfere with ion channeling. Positron annihilation lifetime spectroscopy has been used in semiconductors to study irradiation-induced vacancies. Anion vacancies in alkali halides and alkaline earth oxides give rise to optical absorption from F centres that can be detected using cathodoluminescence (CL) or electron spin resonance (ESR) if they contain unpaired electron spins. In this study, alkaline earth titanates were monitored using time resolved CL spectroscopy.

* Corresponding author. Tel.: +61-2 9717 3505; fax: +61-2 9543 7179.

E-mail address: kls@ansto.gov.au (K.L. Smith).

0022-3115/01/$ - see front matter
PII: S0022-3115(00)00698-X

Time resolved CL spectroscopy (TRCS) involves irradiating the sample with fast electrons (0.2–0.6 MeV) and monitoring the ultraviolet/visible luminescence produced by short-lived F type centres. For relativistic particles such as electrons, the maximum energy T_m (in eV) transferable from an incident electron of energy E (in MeV) to a lattice ion of mass number A is given [7] by:

$$T_m = 2147.7E(E + 1.022)/A. \quad (1)$$

Consequently, it is possible to determine whether or not atomic displacement occurs upon irradiation by monitoring the change in emission as a function of incident electron energy. If a threshold is observed to occur at incident electron energy E, then the energy T_m is equal to the displacement energy E_d of the atom or ion in the lattice. TRCS has been successfully used to determine the E_d values of various oxides including CaO [8] and MgO [9].

The creation of F-type centres in alkaline earth oxides, single anion vacancies (F^{2+}) produced by displacements which then capture one or two electrons (F^+ and F centres, respectively), results in the production of characteristic luminescence upon excitation by high-energy photons. The creation process can be represented by:

$$F^{2+} + e \rightarrow F^+$$

$$F^{+*} \rightarrow F^+ + hv$$

where $*$ denotes an excited state. In CaO for example, the 375 nm emission band has been shown [10] to occur from the relaxation of an excited F^+ centre. The 380 nm emission in MgO has been assigned to a similar centre. More recently [11,12], the 330 nm emission in sapphire (Al_2O_3) has also been ascribed to an F^+ centre relaxation.

2. Experimental

The single crystal perovskite samples used in this study were $2 \times 2 \times 10$ mm^3 slices of high-quality single crystals (originally $2 \times 10 \times 10$ mm^3 in size) purchased from Escete (Netherlands). The polycrystalline $CaTiO_3$ sample was made via the alkoxide/nitrate route [1] and sintered in air at 1400°C.

A Febetron 706 (Hewlett Packard, Field Emission Division) pulsed electron beam generator was used at room temperature to irradiate the samples. Pulses of electrons of duration 3 ns (FWHM) and a designated energy from 0.2–0.6 MeV could be produced. The energy of the designated electron energies is accurate to within 5–10%, as determined by beam penetration through gold and aluminium foils of known thickness. The maximum output of the Febetron at 0.6 MeV is 12 J. The diameter of the electron beam was ~2 cm. The relative dose per pulse delivered by the electron accelerator was calibrated at intervals over the energy range 0.2–0.6 MeV using a 'radiochromic' dosimetry technique [13]. The calibrations were fitted to an appropriate spline function, which was then used to interpolate doses at intermediate beam energies.

The light emission from the sample was observed at 90° to the axis of the electron beam via a system of quartz lenses focussing onto the slits of a monochromator (Spex Industries, Minimate 1670). Typically, a bandpass of 2 nm was used to record emission spectra, and 5 nm was used for threshold determinations. This latter condition allowed greater sensitivity at low electron beam energies. For emission spectra that show no sharp features, this procedure is valid.

The sample was mounted centrally in front of the electron beam window, with the [1 0 0] face at approximately 45° to the axis of the electron beam. Consequently, the electron irradiations were not along any specific crystallographic direction. The beam was collimated to about 6 mm diameter, which was usually greater than the dimensions of the sample. The crystal and mount were contained in an aluminium vessel equipped with high purity quartz windows through which emissions from the irradiated crystal could be observed. The irradiation vessel was mounted directly on to the front of the Febetron and was routinely evacuated to less than 10^{-3} Torr prior to irradiation. This procedure was followed to eliminate emissions from components in air (mainly N_2 and H_2O fragments), which occur in the 300–400 nm region of the spectrum and have comparable lifetimes to those anticipated for F-type luminescent defects.

The output from the optical system was monitored with a photomultiplier (EMI, 9783B), displayed on a digitizing/digital oscilloscope (Tektronix, TDS 744A) and exported to a Macintosh Quadra PC for further analysis. The risetime of this system was of the order of 10 ns. The time between pulses at different wavelengths or energies was about 30 s.

Photoluminescence (PL) measurements of $CaTiO_3$ and $SrTiO_3$, irradiated with the Febetron were made using a Perkin Elmer LS 50 Photoluminscence Spectrometer. PL spectra were corrected for system response.

3. Results

In all samples, light emission was observed immediately after the electron beam pulse (see Fig. 1), if the pulse energy was greater than the displacement threshold. The emission had a rapid initial decay over a period of 50 ns but the decay merged into a long 'tail' which continued for a period of many microseconds. The

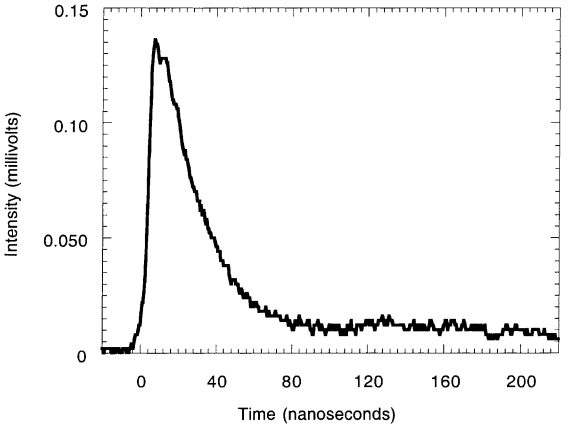

Fig. 1. Intensity of light (at 390 nm) emitted from a $CaTiO_3$ perovskite sample irradiated at room temperature as a function of time.

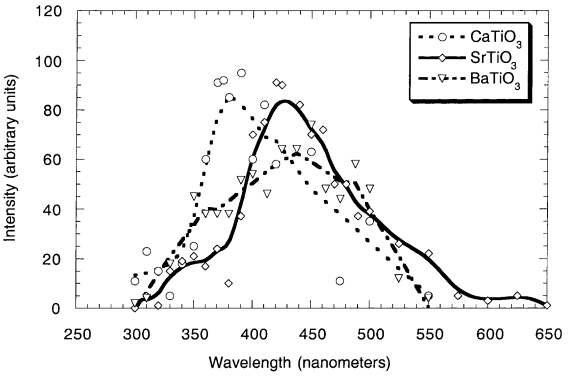

Fig. 2. Room temperature luminescence spectra from single crystal $CaTiO_3$, $SrTiO_3$ and $BaTiO_3$.

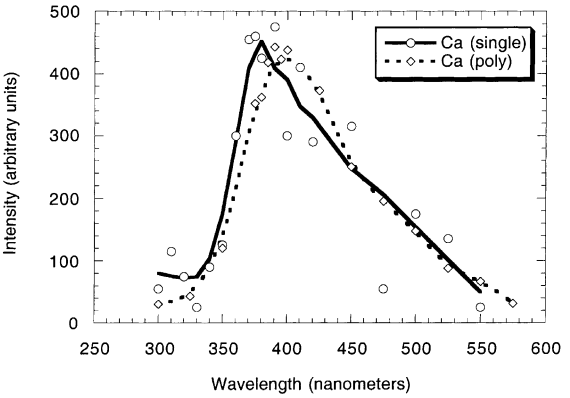

Fig. 3. Comparison of room temperature luminescence spectra from single crystal and polycrystalline $CaTiO_3$.

decay of emission did not follow a simple decay. This is typical of solid state dispersion kinetics behaviour, which involves a distribution of centres participating in recombination processes leading to luminescence [14]. This model gives rise to a power law time dependence of intensity (intensity is proportional to time^{-y}, where y is in the range 1–2, as per Fig. 1).

Over the electron energy range used in this study, the time-dependent profile of the emission did not discernibly change. This means that the observation of a single intensity at a fixed time after the pulse is directly proportional to the integrated light yield. In this study, wavelength-dependent spectra were recorded by measuring the intensity of emission 25 ns after the electron beam pulse. Three measurements were made at each wavelength. The wavelength range scanned was usually from 300 to 600 nm depending on the specific spectral features. Recordings were made at 10 nm intervals, except around emission maxima where some readings were taken at 5 nm intervals. The shape and intensity of the spectra did not depend on the order in which data was taken. This suggests electron irradiation causes no observable permanent defect concentrations.

Fig. 2 shows the spectra recorded at room temperature for single crystal specimens of $CaTiO_3$, $SrTiO_3$ and $BaTiO_3$. The maximum emissions for $CaTiO_3$, $SrTiO_3$ and $BaTiO_3$ occur at around 380, ~420 and ~445 nm, respectively. This distinct shift towards longer wavelengths occurs as calcium is replaced with successively heavier alkaline earth cations.

A sample of polycrystalline $CaTiO_3$, of similar overall size to the single crystal $CaTiO_3$ sample, was also irradiated at room temperature using the Febetron. The emission intensity and spectra of the polycrystalline sample are essentially identical to those of the $CaTiO_3$ single crystal (Fig. 3). This indicates that emission from surface damage sites or at grain boundaries is not a significant factor and that the emission is from sites located within the bulk of the material. However, the grain size was ~10 μm and so the grain boundary scattering would dictate that the emission was mostly derived from a surface layer no more than ~10 μm thick.

Fig. 4 shows the emission yield per dose versus the electron beam energy at room temperature for the four samples studied. All the samples show a distinct threshold for the onset of the emission at around 0.26 MeV. Within experimental error, all four curves shown can be interpreted as having a common intercept of 0.26 ± 0.02 MeV. Using Eq. (1) and assuming oxygen ion displacement, this gives a value for the displacement energy of oxygen, E_d (oxygen), of 45 ± 4 eV. Because of the random orientation of the single crystals and the overall agreement with the polycrystalline results for $CaTiO_3$, the measured displacement energies are likely the overall minimum threshold displacement energies for these perovskites.

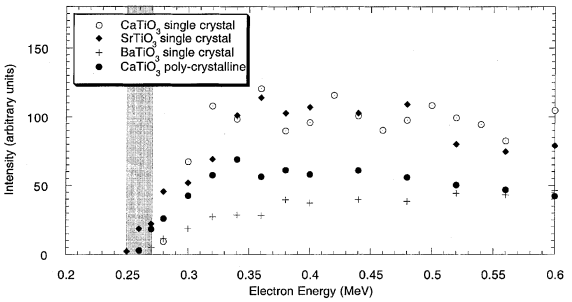

Fig. 4. Graphs of the intensity emitted by $CaTiO_3$, $SrTiO_3$ and $BaTiO_3$ at room temperature as a function of energy.

We measured the room temperature PL due to residual defects in irradiated $CaTiO_3$ and $SrTiO_3$. The signals are weak, indicating very low permanent defect concentrations, in agreement with the deductions stated above.

4. Discussion

The prompt CL observed in our pulsed experiments is similar in wavelength dependence to that seen in steady irradiation experiments reported by Ihrig et al. [15]. Using a continuous 25 keV electron beam, they recorded the luminescence spectra of $SrTiO_3$ and $BaTiO_3$ after various pre-treatments. Low energy (<30 keV) electron beams are not able to generate atom/ion displacements but will excite existing F-type centres. All the samples studied by Ihrig et al. showed emission spectra over the 350–600 nm range with partially resolved peaks in the 400–500 nm region. Samples that were pre-treated in a reducing atmosphere gave the largest CL signals because of the large concentrations of F-type centres they contained. The spectra Ihrig et al. collected from reduced $SrTiO_3$ and $BaTiO_3$ show a similar shift in wavelength to that observed between the $SrTiO_3$ and $BaTiO_3$ spectra collected in this study.

Weber et al. [16] saw significant annealing of oxygen vacancies in $SrTiO_3$ at temperatures between 200 and 400 K, in agreement with our PL results, which demonstrates that room temperature electron irradiation of $CaTiO_3$ and $SrTiO_3$ causes negligible quantities of permanent defects.

Zinkle and Kinoshita [17] collated all available E_d data for Al_2O_3, MgO, $MgAl_2O_4$, ZnO, UO_2, and BeO including those measured using optical absorption, TEM (loops), luminescence, resistivity and ESR. The threshold values and E_d(oxygen) values calculated from the data measured in this study are similar to: (a) the E_d(oxygen) values recommended by Zinkle and Kinoshita [17] for MgO and Al_2O_3, and (b) those determined by TRCS for oxygen in other oxides (see Table 1).

Table 1
Comparsion of oxygen coordination, oxygen–metal bond lengths and E_d(oxygen) values in various oxides

Material formula/ oxygen site	Coordination of oxygen site	Bond type	Bond lengths[a] (Å)	Average bond length (Å)	E_d(oxygen) (eV)
CaO[b]	6	O–Ca	6×2.4053	2.4053	58 ± 2[c]
MgO[d]	6	O–Mg	6×2.1085	2.1085	50[e], 55 ± 2[c]
Al_2O_3[f]	4	O–Al	2×1.8554 and 2×1.9724	1.9124	50[e], 49 ± 2[c]
Perovskite [g]	6	O(1)–Ca	2.4669, 2.5000, 2.8955 and 2.9877	2.4493	45 ± 4[h]
$CaTiO_3$/O(1)		O(1)–Ti	1.9228, 1.9228		
Perovskite[g]	5	O(2)–Ca	2.5519, 2.5838 and 2.6844	2.3345	45 ± 4[h]
$CaTiO_3$/O(2)		O(2)–Ti	1.9244 and 1.9280		
Perovskite[i]	6	O–Sr	4×2.7613	2.4917	45 ± 4[h]
$SrTiO_3$		O–Ti	2×1.9525		
Perovskite[g]	6	O(1)–Ba	4×2.8290	2.5557	45 ± 4[h]
$BaTiO_3$/ O(1)		O(1)–Ti	1.8724 and 2.1456		
Perovskite[g]	6	O(2)–Ba	2×2.8778	2.5581	45 ± 4[h]
$BaTiO_3$/ O(2)		O(2)–Ti	2×2.7923 and 2×2.0043		

[a] As calculated by 'CrystalMaker 4.0', a Mac based PC program for drawing and analysing crystallographic structures.
[b] F.D. Bloss, 'Crystallography and Crystal Chemistry', Holt Rinehart and Winston, USA (1971) 241.
[c] Values measured by 11.
[d] Sasaki S, Fujino K, Takeuchi Y, Proceedings of the Japan Academy, 55 (1979) 43.
[e] Values recommended by Zinkle and Kinoshita [17].
[f] Finger and Hazen, J. Appl. Phys. 49 (1978) 5823.
[g] Wyckoff R.W.G., Crystal Structures, 2nd ed., Interscience, New York, Vols. 1–3, 1981–86.
[h] Values measured in this study.
[i] Megaw, Helen D., 'Crystal structures: a working approach', Studies in physics and chemistry; No. 10. Philadelphia: Saunders, 1973, p. 217.

We considered the possibility that E_d(oxygen) values in oxides are affected by the number and strength of the bonds that oxygen ions have with neighbouring metal ions. As bond length is an indicator of bond strength, we calculated the number and proximity of metal ions around oxygen ions in perovskite and various other oxides and compared these values with the corresponding E_d (oxygen) values (Table 1). The data in Table 1 show that the E_d of oxygen in close packed oxide ion lattices is of the order of 50 eV, regardless of the local environment in which the oxygen ion is located.

5. Conclusion

In this study, the threshold of fast-electron (0.2–0.6 MeV) induced ultraviolet/visible fluorescence was used to determine the E_d values of oxygen in three alkaline earth titanates at room temperature. On the basis that the observed thresholds were due to oxygen displacements, the E_d of oxygen in $CaTiO_3$, $SrTiO_3$ and $BaTiO_3$ was found to be 45 ± 4 eV. This is comparable to the E_d values of oxygen in other oxides. Further work is necessary to more accurately define the shape of the optical emission bands.

References

[1] A.E. Ringwood, S.E. Kesson, N.G. Ware, W. Hibberson, A. Major, Nature (London) 278 (1979) 219–223.
[2] W.J. Weber, R.P. Turcotte, F.P. Roberts, Radioactive Waste Manage. 2 (1982) 295–319.
[3] H. Mitamura, S. Matsumoto, M.W.A. Stewart, T. Tsuboi, M. Hashimoto, E.R. Vance, K.P. Hart, Y. Togashi, H. Kanazawa, C.J. Ball, T.J. White, J. Amer. Ceram. Soc. 77 (1994) 2255–2264.
[4] E. Vernaz, A. Loida, G. Malow, J.A.C. Marples, Hj. Matzke, in: Presented at 3rd European Community Conference on Radioactive Waste Management and Disposal, Luxembourg, 17–21 September 1990.
[5] K.L. Smith, N.J. Zaluzec, G.R. Lumpkin, J. Nucl. Mater. 250 (1997) 36–52.
[6] K.L. Smith, G.R. Lumpkin, M.G. Blackford, N.J. Zaluzec, Mater. Res. Soc. Symp. Proc. 540 (1999) 323–329.
[7] E. Sonder, W.A. Sibley, in: J.H. Crawford Jr., L.M. Slifkin (Eds.), Point Defects in Solids, Vol. I, Plenum, New York, 1972, p. 201.
[8] J.L. Grant, R. Cooper, J.F. Boas, J. Chem. Phys. 88 (1988) 4158–4170.
[9] J.L. Grant, R. Cooper, P. Zeglinski, J.F. Boas, J. Chem. Phys. 90 (1989) 807–812.
[10] B. Henderson, CRC Crit. Rev. Solid State Mater. Sci. 9 (1980) 1–60.
[11] K.J. Caulfield, R. Cooper, J.F. Boas, J. Amer. Ceram. Soc. 78 (1995) 1054–1060.
[12] B.D. Evans, M. Stapelbroek, Phys. Rev. B 18 (1978) 7089–7098.
[13] K.C. Humphreys, A.D. Kantz, Radiat. Phys. Chem. 9 (1977) 737–747.
[14] K.J. Caulfield, R. Cooper, J.F. Boas, J. Phys.: Condens. Mater. 9 (1997) 6457–6465.
[15] H. Ihrig, J.H.T. Hengst, M. Klerk, Z. Phys. B 40 (1981) 301–306.
[16] W.J. Weber, W. Jiang, S. Thevuthasan, R.E. Williford, A. Meldrum, L.A. Boatner, in: G. Borstel, A. Krumins, D. Miller (Eds.), Defects and Surface-induced Effects in Advanced Perovskites, Kluwer Academic Publishers, Netherlands, 2000, pp. 317–328.
[17] S.J. Zinkle, C. Kinoshita, J. Nucl. Mater. 251 (1997) 200–217.